JVI Journals.ASM.org

The Influenza Virus Neuraminidase Protein Transmembrane and Head Domains Have Coevolved

Diogo V. da Silva,[a] Johan Nordholm,[a] Dan Dou,[a] Hao Wang,[a] Jeremy S. Rossman,[b] Robert Daniels[a]

Center for Biomembrane Research, Department of Biochemistry and Biophysics, Stockholm University, Stockholm, Sweden[a]; School of Biosciences, University of Kent, Canterbury, United Kingdom[b]

ABSTRACT

Transmembrane domains (TMDs) from single-spanning membrane proteins are commonly viewed as membrane anchors for functional domains. Influenza virus neuraminidase (NA) exemplifies this concept, as it retains enzymatic function upon proteolytic release from the membrane. However, the subtype 1 NA TMDs have become increasingly more polar in human strains since 1918, which suggests that selection pressure exists on this domain. Here, we investigated the N1 TMD-head domain relationship by exchanging a prototypical "old" TMD (1933) with a "recent" (2009), more polar TMD and an engineered hydrophobic TMD. Each exchange altered the TMD association, decreased the NA folding efficiency, and significantly reduced viral budding and replication at 37°C compared to at 33°C, at which NA folds more efficiently. Passaging the chimera viruses at 37°C restored the NA folding efficiency, viral budding, and infectivity by selecting for NA TMD mutations that correspond with their polar or hydrophobic assembly properties. These results demonstrate that single-spanning membrane protein TMDs can influence distal domain folding, as well as membrane-related processes, and suggest the NA TMD in H1N1 viruses has become more polar to maintain compatibility with the evolving enzymatic head domain.

IMPORTANCE

The neuraminidase (NA) protein from influenza A viruses (IAVs) functions to promote viral release and is one of the major surface antigens. The receptor-destroying activity in NA resides in the distal head domain that is linked to the viral membrane by an N-terminal hydrophobic transmembrane domain (TMD). Over the last century, the subtype 1 NA TMDs (N1) in human H1N1 viruses have become increasingly more polar, and the head domains have changed to alter their antigenicity. Here, we provide the first evidence that an "old" N1 head domain from 1933 is incompatible with a "recent" (2009), more polar N1 TMD sequence and that, during viral replication, the head domain drives the selection of TMD mutations. These mutations modify the intrinsic TMD assembly to restore the head domain folding compatibility and the resultant budding deficiency. This likely explains why the N1 TMDs have become more polar and suggests the N1 TMD and head domain have coevolved.

Receptors on the surface of cells and enveloped viruses are often comprised of single-spanning (bitopic) membrane proteins. The majority of the structures for these proteins exclude their transmembrane domain (TMD), which has hindered the ability to identify any potential contributions of the TMD to protein folding and activity. Instead, studies with model and natural TMD segments in reductionist systems have been used to determine how they interact (reviewed in references 1–3). The biological functions of these TMD interactions in bitopic proteins are much less characterized and have been linked mainly to oligomerization and activity (4–9). The current challenge is to better define the plasticity of bitopic TMD interactions and how they contribute to protein folding and activity in native biological systems.

Enveloped viruses, which have been used to identify and investigate numerous cellular pathways and processes (10–13), are an ideal system to address these questions. Generally, a significant amount of sequence data is available for enveloped viruses that infect mammalian cells, and they normally carry one or more bitopic membrane proteins with a known function (14, 15). In addition, viral reverse genetic approaches provide the ability to test the biological implications of TMD changes *in vivo*, and viral replication often selects for viable compensatory mutations that can be identified by viral genome sequencing.

Recently, we have exploited these features to examine the type II membrane protein neuraminidase (NA) from influenza A viruses (IAVs). Two NA subtypes (N1 and N2) exist in human IAVs, and both form homotetramers with an enzymatic head domain connected by a stalk to an N-terminal TMD (Fig. 1A). The TMD targets NA to the endoplasmic reticulum and facilitates its membrane integration and transport to the plasma membrane, where the head domain then cleaves off the IAV cell surface receptor (sialic acid) to promote virus release (16–18). Since the NA head domain retains its enzymatic activity upon proteolytic cleavage off the viral membrane, its TMD is thought to function primarily as a membrane anchor (19).

However, we previously showed that the N1 TMD uses polar residues to independently form an amphipathic tetramer that sta-

Received 11 July 2014 **Accepted** 26 October 2014

Accepted manuscript posted online 5 December 2014

Citation da Silva DV, Nordholm J, Dou D, Wang H, Rossman JS, Daniels R. 2015. The influenza virus neuraminidase protein transmembrane and head domains have coevolved. J Virol 89:1094–1104. doi:10.1128/JVI.02005-14.

Editor: A. García-Sastre

Address correspondence to Robert Daniels, robertd@dbb.su.se.

Supplemental material for this article may be found at http://dx.doi.org/10.1128/JVI.02005-14.

doi:10.1128/JVI.02005-14

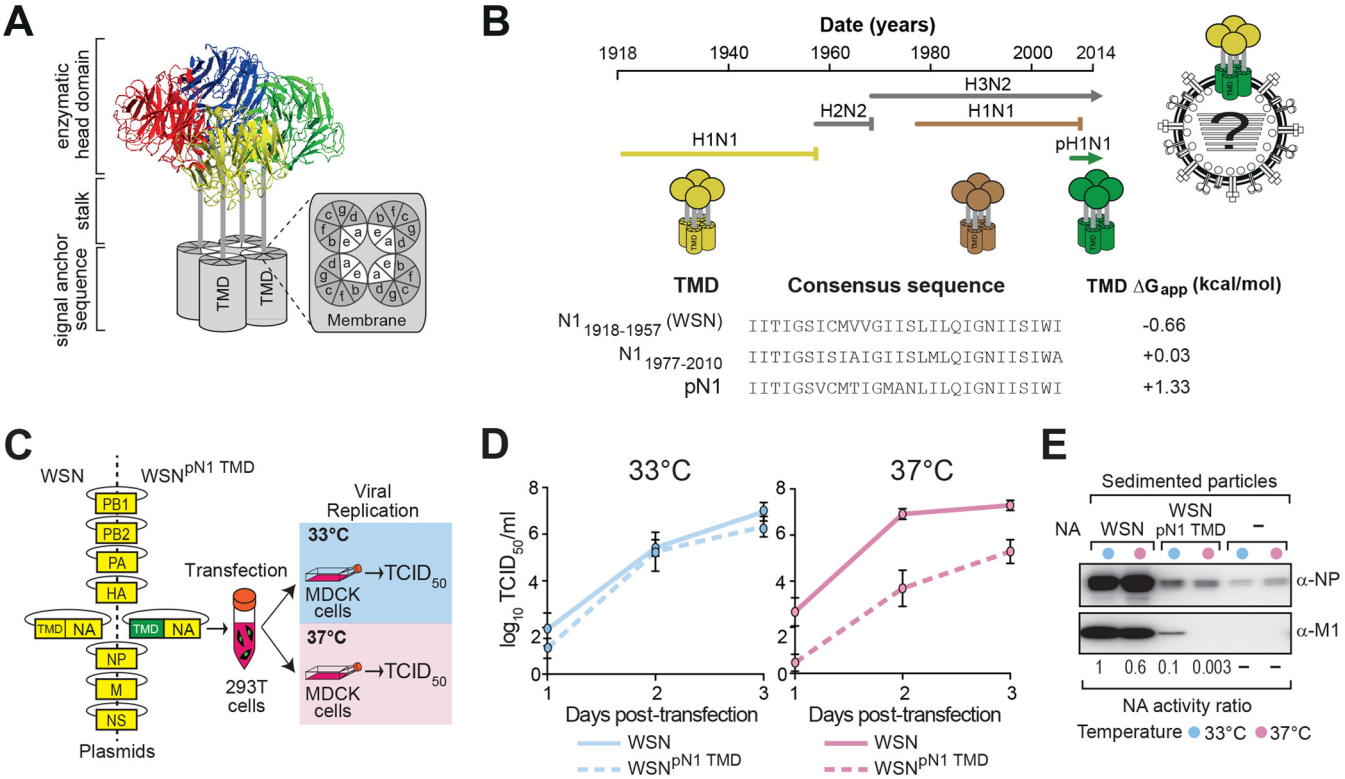

FIG 1 A recent N1 TMD impairs the replication of an old H1N1 virus at 37°C. (A) The three domains of an NA tetramer are shown with the 7-face TMD model for its amphipathic assembly via the polar faces *a* and *e* (21). (B) The timeline depicts the different human IAV lineages by their hemagglutinin (H) and neuraminidase (N) subtypes with the predicted hydrophobicity values (ΔG_{app} values for membrane insertion) of the consensus N1 TMD sequences for the H1N1 lineages. (C) Split-transfection method for comparative viral production by reverse genetics. Trypsinized 293T cells are transfected with WSN plasmids encoding its old N1 TMD or the recent pN1 TMD, divided into flasks containing MDCK cells at 33°C and 37°C, and viral titers are assayed by $TCID_{50}$ values. (D) The recent pN1 TMD significantly decreases the replication of the 1933 H1N1 virus WSN at 37°C compared to at 33°C. The viral titers are displayed as means from three independent experiments ± standard errors of the means (SEM). (E) WSN and $WSN^{pN1\text{-}TMD}$ viral particles created by reverse genetics were isolated from the culture medium 3 days after recovery by ultracentrifugation. The M1 and NP contents were assayed by immunoblotting and the NA content by activity, which is displayed as a ratio to the WSN sedimented particles from 33°C. Cells that did not receive the NA plasmid were used as a control.

bilizes the stalk and allows the head domain to fold (Fig. 1A [*a* and *e* are the polar faces of the TMD model]) (20, 21). Contradictory to the need to conserve hydrophobicity for membrane integration, our analysis of the N1 TMDs in human IAVs showed that they have become increasingly more polar since 1918, which results in a stronger TMD association (21). These findings suggest the N1 TMD is potentially evolving to compensate for the selective evolutionary changes in the enzymatic head domain that likely affect its folding, as recent N1's have been shown to possess lower enzymatic activity (22).

Here, we manipulated the NA TMD hydrophobicity and assembly in an "old" prototypical H1N1 virus and exploited the replication and mutation capacity of the virus to investigate the impact of these TMD changes in a biological context. Our results show that the relationship between the NA TMD and enzymatic head domain is critical for viral budding and replication and that IAVs select for rescue mutations in the TMD. These mutations strongly correlate with the mechanism of TMD assembly (e.g., polar substitutions in amphipathic TMDs and hydrophobic substitutions in hydrophobic nonamphipathic TMDs) and restore the folding efficiency of the distal NA head domain and subsequently viral budding. Our findings demonstrate that TMDs can significantly influence the folding and function of distal domains in bitopic proteins and suggest that N1 TMDs in human influenza viruses have altered their intrinsic polar assembly properties to compensate for changes in the head domain.

MATERIALS AND METHODS

Plasmids. The influenza virus A/WSN/33 (H1N1) eight-plasmid reverse genetics system was used as the backbone for all H1N1 viruses (23). The $WSN^{pN1\text{-}TMD}$ virus was created by using overlap cloning (24) to replace the WSN NA TMD coding sequence with the human pN1 TMD consensus sequence generated from the NCBI Influenza Virus Resource Database (identical in amino acid sequence to A/California/04/09). In this construct, the *a* face Asn residues at positions 21 and 28 in the pN1 TMD were mutated to Ala to produce the pN1 TMDΔA chimera. For individual analysis, full-length NA (from WSN) and the pN1 TMD and pN1 TMDΔA chimeras were fused to the C-terminal Myc-His tag in the mammalian expression vector pcDNA3.1A-Myc-His (Invitrogen) by PCR overlap cloning as previously described (20). The pBLM plasmids, used for TMD interaction studies, containing the NA TMDs are previously described (21). All the TMD mutations in the different constructs were introduced by site-directed mutagenesis, and sequencing was used to verify the plasmids before use (Eurofins MWG Operon).

Cell culture and individual NA transfections. MDCK and HEK 293T cells, obtained from ATCC, were cultured in Dulbecco's modified Eagle's medium (DMEM; Invitrogen) supplemented with 10% fetal bovine serum (FBS) and 100 U/ml of penicillin and streptomycin (P-S) and kept in

a humidified atmosphere at 33°C or 37°C with 5% CO_2. For each transfection, 3 μg of plasmid DNA was incubated for 20 min with 10 μl of LT-1 (Mirius) in 1 ml of Opti-MEM (Invitrogen). Trypsinized 293T cells were resuspended in Opti-MEM–10% FBS to a cell density of 1×10^6 cells/ml, 2 ml of cells was added to the transfection mixture, and 1.45 ml of the resulting cell and transfection mix was added to two 3.5-cm dishes that were placed at 33°C and 37°C. Forty-eight hours posttransfection, cells were washed with phosphate-buffered saline (PBS), pH 7.4, and collected by scraping in 150 μl of lysis buffer (20 mM Tris [pH 7.4], 150 mM NaCl, 1% *n*-dodecyl β-D-maltoside, 10 mM *N*-ethylmaleimide, 1× protease inhibitor [Sigma]). Lysates were sonicated on ice for 30 s and sedimented (20,000 × *g*, 5 min), and the postnuclear supernatants were retained.

Split-transfection method for IAV production by reverse genetics. WSN, $WSN^{pN1\text{-}TMD}$, and $WSN^{pN1\text{-}TMD\Delta A}$ viruses were generated at 33°C and 37°C by an altered version of the standard eight plasmid protocol (23). First, MDCK cells were harvested by trypsinization and resuspended to a density of 1×10^6 cells/ml in Opti-MEM–10% FBS. For each virus, 1.5 ml of MDCK cells was added to two 25-cm^2 flasks, which were placed in incubators at 33°C or 37°C. Next, 1 μg of each of the eight plasmids (the NA plasmid was exchanged for the different chimeras) was mixed in 1.5 ml of Opti-MEM with 20 μl of LT-1 and incubated for 20 min in a 15-ml tube. After the incubation, 293T cells were trypsinized, sedimented (500 × *g*, 3 min), and resuspended to a density of 1×10^6 cells/ml in Opti-MEM, and 1.5 ml of cells was added to the plasmid transfection mixture and incubated for 15 min. The 3-ml mixture was then split, and 1.45 ml was added to the MDCK cell flasks at 33°C and 37°C. A sample was taken 24 h posttransfection, and the medium was then replaced with 3 ml infection medium (DMEM with 0.1% FBS, 0.3% bovine serum albumin [BSA], 1% P-S, and 2.5 μg/ml of TPCK trypsin) and incubated for an additional 48 h, with samples taken every 24 h.

Viral titer determination, passaging, and sedimentation. Viral titers at 24, 48, and 72 h posttransfection were determined by titration on MDCK cells and calculated as the median tissue culture infectious dose ($TCID_{50}$) per milliliter at 33°C or 37°C, matching the temperature at which the virus was generated. The final titers were determined by the observation of cytopathic effects (CPE) at 72 h according to reference 25. For viral passaging, confluent monolayers of MDCK cells cultured at 33°C and 37°C were infected with the recombinant viruses generated at the same temperature using a multiplicity of infection (MOI) of ~0.001. At day 3, the viral supernatant was isolated, the titer was determined, and this procedure was repeated for the indicated number of passages. To isolate the viral particles, 1 ml of culture medium from 72 h posttransfection was sedimented for 5 min at 10,000 × *g*, and 800 μl of the supernatant was layered on top of a 400-μl sucrose cushion (100 mM Tris [pH 7.4], 150 mM NaCl, 0.63 M sucrose). After sedimentation for 45 min at 70,000 × *g*, the supernatant was removed and the viral particles were resuspended in 150 μl of lysis buffer.

NA activity assay and immunoblotting. Sialidase activity was determined for each NA sample panel prior to immunoblotting by mixing 5 μl of postnuclear supernatants with 190 μl of reaction buffer (0.1 M potassium phosphate [pH 6.0], 1 mM $CaCl_2$). Reactions were initiated with 5 μl of 2 mM 2′-(4-methylumbelliferyl)-α-D-*N*-acetylneuraminic acid (Sigma), and the activity was determined as previously described using the linear range of the 450-nm emission spectra over 30 min using a SpectraMax Gemini EM (20). Samples were then diluted with untransfected cell postnuclear supernatant to equivalent activity levels. Equal amounts were mixed 1:1 with nonreducing or reducing (0.1 M dithiothreitol [DTT]) Laemmli sample buffer, heated to 37°C for 10 min, resolved by SDS-PAGE, and transferred to a polyvinylidene difluoride (PVDF) membrane (26). Membrane processing has previously been described (20). The folding efficiency was determined by normalizing the sialidase activity to the respective band intensity of the sample from a reducing immunoblot, with the value obtained for NA^{WSN} at 33°C set to 100%. For bacterial samples, an A_{600} value of 1 for *Escherichia coli* was sedimented (5,000 × *g*, 5 min), directly resuspended in reducing Laemmli sample buffer, and sonicated prior to SDS-PAGE.

RNA extraction, PCR amplification, and sequencing. Virus-containing medium was harvested ~72 h posttransfection or postinfection and clarified by sedimentation (5,000 × *g*, 5 min), and the supernatant was layered on top of a 20% sucrose cushion (100 mM NaCl, 10 mM Tris-Cl [pH 7.4]) and sedimented (130,000 × *g*, 40 min, 4°C) in a Beckman TLA 100.2 rotor. Viral RNAs were extracted from the viral pellet with the RNeasy minikit (Qiagen). cDNAs were generated with the AffinityScript multiple temperature cDNA synthesis kit (Agilent) with a primer complementary to the conserved 3′ end of the viral RNAs. The NA, hemagglutinin (HA), and matrix (M) genes were amplified by PCR, purified with a PCR clean-up column (Promega), sequenced (Eurofins MWG Operon), and analyzed using Lasergene 8.0 software.

TMD interaction measurements. SU101 *E. coli* cells with an *lacZ* gene regulated by an LexA operator (27) were transformed with each pBLM TMD expression plasmid and grown overnight in lysogeny broth (LB) with 100 μg/ml ampicillin. Cultures were back-diluted to an A_{600} value of 0.1 in LB with 100 μg/ml ampicillin and induced with 50 μM isopropyl-β-D-thiogalactopyranoside (IPTG) at 37°C for 2.5 h until an A_{600} value of ≈0.6. The relative interaction strength (RI) was determined by normalizing the β-galactosidase activity from each sample (X_s) to the activity of cells with an empty vector (X_v), where $X_{norm} = X_s/X_v$, and using the formula $RI = 100\%(1 - X_{norm})$.

Sequence analysis and statistics. All NA and M2 protein sequences from the indicated IAV populations were retrieved from the NCBI Influenza Virus Resource Database and separated by their date of isolation, geographic location, and species origin. Predicted hydrophobicities of the TMDs (ΔG_{app}) and each TMD face ($\Delta G_{app\text{-}face}$) were calculated using the ΔG predictor (28) as previously described (21).

RESULTS

A "recent" N1 TMD impairs the replication of an "old" H1N1 influenza virus. Every IAV contains a genome segment that encodes 1 of the 16 hemagglutinin subtypes (H1 to H16) and another which encodes 1 of the 9 neuraminidase subtypes (N1 to N9) (29). In humans, only IAVs with the combinations of H1N1, H2N2, and H3N2 have circulated for extended time periods during the last century (Fig. 1B); this includes two earlier H1N1 lineages (1918 to 1957 and 1977 to 2010) and the current pandemic virus (pH1N1) lineage that began in 2009. From one lineage to the next, surface residues on the N1 head domains have changed due to antigenic pressure, coincident with decreases in TMD hydrophobicity and enzymatic rate (V_{max}) (21, 22). The sequential hydrophobicity decrease is shown by the predicted ΔG_{app} values of membrane insertion (28) for the consensus N1 TMDs from each H1N1 lineage going from negative to more positive (Fig. 1B, −0.6 kcal/mol to +0.03 kcal/mol to +1.3 kcal/mol).

First, we investigated the relationship between the N1 TMD and the head domain by modifying an old H1N1 virus to carry a more polar, recent N1 TMD (Fig. 1B). The well-characterized 1933 H1N1 lab strain, A/WSN/33 (WSN), was chosen as the old background strain because its TMD matches the consensus N1 TMD sequence of the human H1N1 viruses sequenced from 1918 to 1957. In the WSN background, the N1 TMD was exchanged with the consensus N1 TMD sequence from the contemporary pH1N1 viruses to generate the chimera ($WSN^{pN1\text{-}TMD}$).

Next, we created a reproducible split-transfection assay for IAV production by reverse genetics that compares viral replication at 37°C and 33°C to identify NA folding defects that impact viral replication and to control for possible failures in virus recovery (Fig. 1C). The temperature range was based on previous observations that NA-defective viruses can be recovered at 33°C but

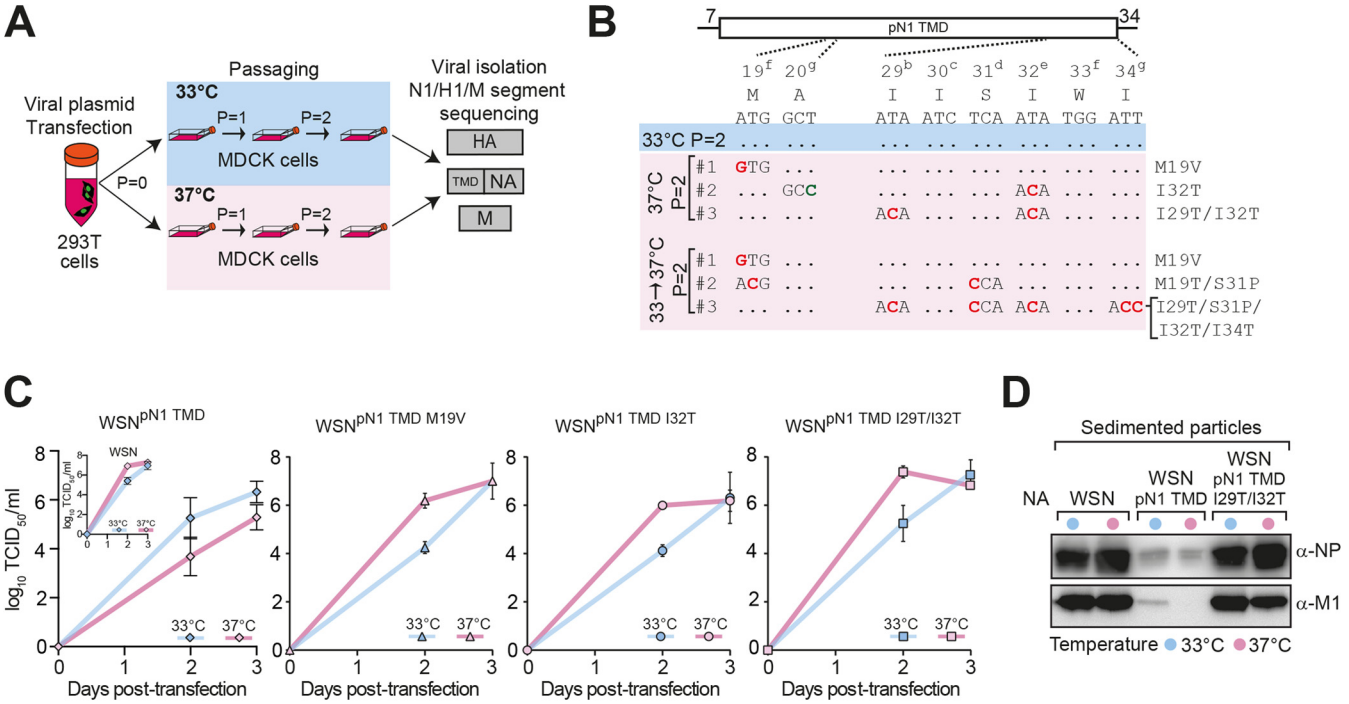

FIG 2 Nonoptimal N1 TMDs are under temperature-dependent selection pressure. (A) Viral passaging and sequencing. MDCK cells at 33°C and 37°C were infected at an MOI of ~0.001 with the WSN and WSN$^{pN1\text{-}TMD}$ viruses generated at 33°C or 37°C for 3 days and repeated for the indicated number of passages (P). For each passage, viruses were isolated 3 days postinfection, and genomes were extracted and sequenced. (B) pN1 TMD mutations were selected for in the WSN$^{pN1\text{-}TMD}$ viruses produced and passaged twice at 37°C (pink box, 37°C P = 2) and when it was produced at 33°C and passaged twice at 37°C (pink box, 33°C to 37°C P = 2). Nonsynonymous (red) and synonymous (green) mutations are displayed with the amino acid number and the TMD face (*a* to *g*). (C) The replication efficiency of WSN$^{pN1\text{-}TMD}$ virus at 37°C was rescued by the virus-selected pN1 TMD mutations (M19V, I32T, and I29T/I32T). Graphs display the mean titers ± SEM at 33°C (blue lines) and 37°C (pink lines) from split transfections of the indicated WSN$^{pN1\text{-}TMD}$ mutants created by reverse genetics. WSN and WSN$^{pN1\text{-}TMD}$ titers from Fig. 1D were included for comparison. (D) Following reverse genetics recovery for 3 days, the indicated viral particles were isolated from the culture medium, and the NP and M1 contents were determined by immunoblotting.

not at 37°C to 39°C, because the folding defects lower the thermal stability of NA (30–32). In this assay, trypsinized 293T cells are transfected with the standard reverse genetics plasmids (23), and the cells are then split and cocultured with MDCK cells (for viral propagation) at 37°C and 33°C. WSN titers provided an additional control, as this virus is known to replicate faster at 37°C than at 33°C (33).

Both the WSN virus and the WSN$^{pN1\text{-}TMD}$ chimera, which carries the recent, more polar pN1 TMD, were generated at 37°C and 33°C (Fig. 1D). Surprisingly, the WSN$^{pN1\text{-}TMD}$ viral titers produced at 37°C were significantly lower than those for WSN, whereas the WSN$^{pN1\text{-}TMD}$ viral titers obtained at 33°C were only slightly lower than those for WSN (Fig. 1D). As expected, WSN replicated faster at 37°C than at 33°C. The fitness loss of the WSN$^{pN1\text{-}TMD}$ virus at 37°C suggests that the recent, more polar pN1 TMD is incompatible with the older WSN head domain, likely resulting in folding defects that are suppressed at the more permissive temperature of 33°C.

The WSN$^{pN1\text{-}TMD}$ virus displays a temperature-dependent budding defect. The drop in the WSN$^{pN1\text{-}TMD}$ viral titer can result from either an increase in defective particle production or a deficiency in viral budding. To discern between these two possibilities, WSN and WSN$^{pN1\text{-}TMD}$ particles from 3 days posttransfection were isolated by ultracentrifugation and examined for their M1, NP, and NA contents (Fig. 1E). Compared to WSN, the WSN$^{pN1\text{-}TMD}$ particles isolated at 37°C and 33°C displayed lower NP levels, and M1 was detected only in the particles isolated at 33°C. While M1 may be below the level of detection for the WSN$^{pN1\text{-}TMD}$ particles isolated at 37°C, the ratio of the NA activities in the isolated particles approximately reflected the differences in the viral infectivity. Together, these data indicate that the lower WSN$^{pN1\text{-}TMD}$ titers are due to a defect in viral budding.

The WSN$^{pN1\text{-}TMD}$ virus selects for N1 TMD mutations to restore replication at 37°C. To gain insight into the potential defect caused by the N1 TMD exchange, we investigated if the WSN$^{pN1\text{-}TMD}$ virus would evolve compensatory mutations. Both WSN and WSN$^{pN1\text{-}TMD}$ viruses were generated at 33°C and 37°C and passaged twice at their respective temperatures in MDCK cells, and the NA TMD region from the resulting viruses was sequenced (Fig. 2A). In three independent trials, at least one mutation appeared in the NA TMD from the WSN$^{pN1\text{-}TMD}$ virus passaged twice at 37°C but not when it was passaged twice at 33°C (Fig. 2B, 37°C P = 2). The WSN virus sequences remained unaltered at both temperatures.

To confirm that the mutations in the pN1 TMD resulted from a replication adaptation at 37°C, WSN$^{pN1\text{-}TMD}$ virus produced at 33°C was passaged twice at 33°C and then passaged two additional times in MDCK cells at 33°C or 37°C. Again, similar mutations appeared in the N1 TMD once the virus was switched to 37°C (Fig. 2B, 33°C to 37°C P = 2), but this approach led to more mixed populations, as each mutation site showed a small peak for the original nucleotide (data not shown). Most of these mutations

were already identified in pure viral populations (Fig. 2B, 37°C P = 2), confirming that replication of the WSN$^{pN1\text{-}TMD}$ virus at 37°C selects for N1 TMD mutations. It should be noted that small peaks for N1 TMD mutations also began to appear in the WSN$^{pN1\text{-}TMD}$ viruses after five passages at 33°C (data not shown), which further indicates that the recent pN1 TMD causes a defect in the older N1 head that is largely suppressed at 33°C.

To check for other potential compensatory mutations, the entire NA, HA, and M segments were also sequenced, because the activity of NA and HA are related, and HA protein maturation involves the M2 ion channel (34–38). In the WSN$^{pN1\text{-}TMD}$ viruses produced at 33°C and 37°C, no substitutions were found in the M segment, and in one experiment, an I265K HA (WSN numbering) mutation was observed that is buried in the receptor binding domain (see Table S1 in the supplemental material). Surprisingly, two of the three WSN$^{pN1\text{-}TMD}$ viruses passaged twice at 33°C acquired mutations (L123F, S156L, and P442T [WSN numbering]) at the oligomeric interface between NA head domain monomers. In contrast, all the WSN$^{pN1\text{-}TMD}$ populations passaged at 37°C contained high frequencies of pN1 TMD mutations at the nucleotide (~2%) and amino acid (~5%) levels, and only one population showed a mutation outside the TMD region in the NA stalk (I68T [WSN numbering]). Thus, WSN$^{pN1\text{-}TMD}$ viruses produced at 37°C preferentially select for mutations in the N1 TMD, while at 33°C, a tendency to select for mutations in the head domain oligomeric interface was observed, which suggested they both may impact NA folding.

The WSN$^{pN1\text{-}TMD}$ viruses were independently generated at 33°C and 37°C with the M19V, I32T, and I29T/I32T pN1 TMD mutations to directly test if they would rescue the replication fitness at 37°C. In all three cases, the TMD mutations restored the faster replication at 37°C and showed replication kinetics comparable to that of WSN (Fig. 2C). Analysis of the isolated WSN$^{pN1\text{-}TMD\ I29T/I32T}$ viral particles confirmed that these mutations also rescued the budding defect as the M1 and NP levels reached those of WSN (Fig. 2D). These results demonstrate a direct relationship between the N1 TMD and head domain sequences and that compatibility between these two domains is required for the proper replication of H1N1 viruses. When this synergistic relationship is disrupted, it appears the head domain drives the selection of compensatory TMD mutations that reestablish the TMD-head domain compatibility.

The WSN$^{pN1\text{-}TMD}$ mutations selected at 37°C make the amphipathic pN1 TMD more polar. N1 TMDs in human H1N1 viruses are amphipathic, and over time they have become more polar (Fig. 1B) (21). The N1 TMDs from the recent pH1N1 viruses are the most polar group with predicted hydrophobicity values ($\Delta G_{app} > 0$ kcal/mol) that are not favorable for membrane insertion (28). This explains our recent finding of why these TMDs depend on cotranslational membrane insertion for their integration and inversion (39). Based on these observations, it was quite unexpected to discover that the WSN$^{pN1\text{-}TMD}$ virus adapted to growth at 37°C by predominantly selecting for polar substitutions that further decreased the predicted TMD hydrophobicity (Fig. 3A, TMD ΔG_{app} trend with increasing positive values). The mutations from the heterogeneous mutant virus populations (e.g., M19T/S31P and I29T/S31P/I32T/I34T) were included as a group and independently, to show the bias and variety of adaptive polar mutations.

We previously showed that consensus N1 TMDs from the three human H1N1 IAV lineages form stable amphipathic tetramers of various hydrophobicity levels (21). The association of the tetramers is driven by a hydrogen bond network created between the adjacent polar *a* and *e* faces of the N1 TMD (Fig. 1A). Therefore, each mutation was analyzed for its effect on the hydrophobicity of the TMD faces (Fig. 3A, $\Delta G_{app\text{-}face}$). The polar substitutions localized to the highly polar *e* face (I32T), the neighboring interfaces *b* (I29T) and *d* (S31P), and their adjacent faces *f* (M19T) and *g* (I34T). The high tendency for polar mutations and the variation of their placement within the TMD suggest these mutations could change the TMD packing by altering the hydrogen bond network in the membrane (40).

pN1 TMD mutations alter the intrinsic association properties to match the WSN N1 TMD. To determine if the polar residue substitutions altered the pN1 TMD assembly, the association of the WSN N1 TMD was compared with the pN1 TMD containing the adapted mutations using the *E. coli* GALLEX system (27). In this system, the interaction strength of the TMDs is measured within the *E. coli* inner membrane by the suppression of β-galactosidase expression and activity. Surprisingly, all the adaptive mutations (M19V, I32T, and I29T/I32T) lowered the relative pN1 TMD association level to that of the WSN N1 TMD, even though the mutations made the TMD more polar and caused further sequence divergence (Fig. 3B). All of the NA TMD constructs were expressed at comparable levels, indicating the change in β-galactosidase expression reflected a decrease in the TMD association. Together, these results indicate that the WSN virus selected for pN1 TMD mutations that modified its intrinsic polar assembly properties to achieve an association level that is compatible with the old N1 head domain in WSN.

NA head domain folding depends on the TMD compatibility. We previously showed that the N1 TMD contributes to head domain folding by stabilizing the stalk in a tetrameric conformation (20), and the WSN$^{pN1\text{-}TMD}$ virus at 33°C showed a tendency to acquire mutations in the N1 head domain oligomeric interfaces (see Table S1 in the supplemental material). This indicated that the recent pN1 TMD likely impairs viral budding by causing a folding defect in the older N1 head domain from WSN that is more pronounced at 37°C. To address this question, the folding of NA from WSN and the NA chimeras WSN$^{pN1\text{-}TMD}$ and WSN$^{pN1\text{-}TMD}$ with the adaptive mutations were compared in 293T cells at 33°C and 37°C. Forty-eight hours posttransfection, the lysates were harvested and analyzed by nonreducing (NR) and reducing (RD) SDS-PAGE to determine the folded (NR) and total (RD) protein levels (Fig. 3C). The folding efficiency was then determined by normalizing the sialidase activity to total protein levels.

All of the NA constructs, except the WSN$^{pN1\text{-}TMD\ M19V}$ rescue mutant at 37°C, were found to fold more efficiently at 33°C than at 37°C, validating that NA generally folds better at 33°C (Fig. 3D and E). The NA chimera, WSN$^{pN1\text{-}TMD}$, showed the lowest folding efficiency at 37°C, which correlated with the decreased WSN$^{pN1\text{-}TMD}$ replication at 37°C. In support of this notion, each mutation in the pN1 TMD that rescued the virus at 37°C also increased the NA folding efficiency of WSN$^{pN1\text{-}TMD}$ at 37°C. Interestingly, the mutations enhanced the NA folding efficiency to various degrees at both 33°C and 37°C, implying there may be a threshold of properly folded NA required for efficient viral replication.

Together, these results demonstrate that folding of the N1 head domain is TMD and temperature dependent and that the compat-

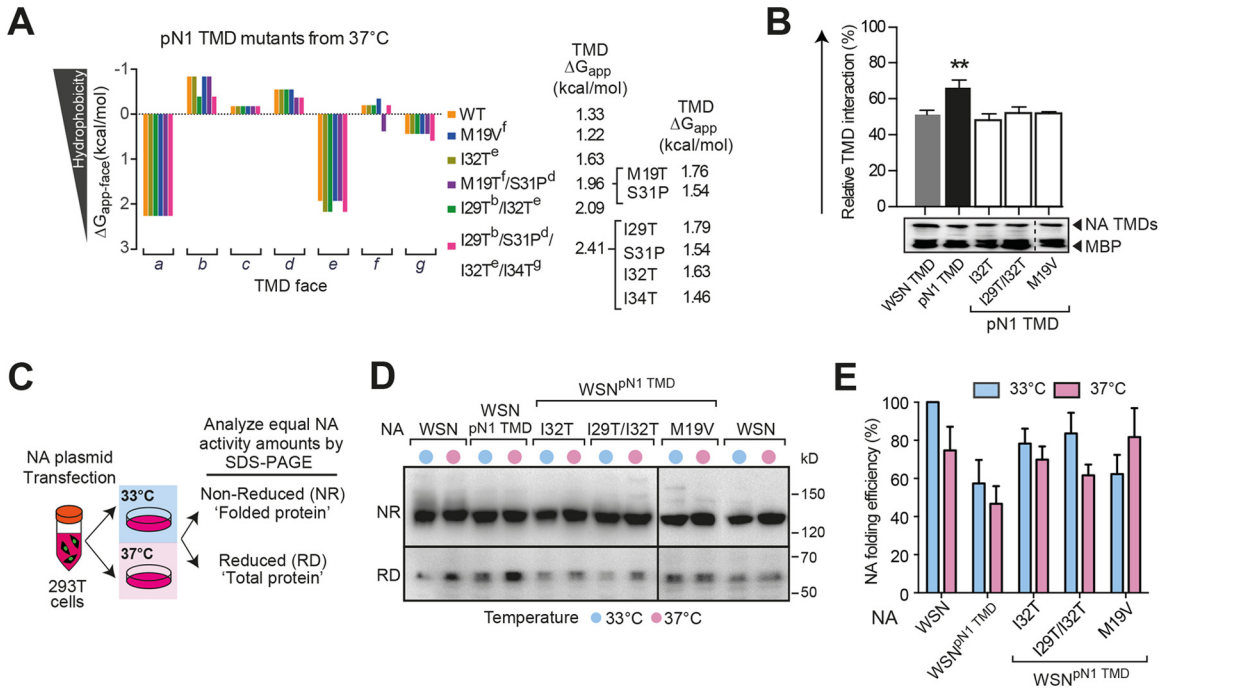

FIG 3 Head domain folding drives the selection of the polar pN1 TMD mutations. (A) The adaptive mutations localize to different faces of the amphipathic pN1 TMD and are mainly polar residues that decrease the face and TMD hydrophobicity (increase the ΔG_{app} values). Predicted ΔG values of the heterogeneous TMD sequences are also displayed independently. (B) The mutations decrease the strong pN1 TMD association to the moderate levels of the N1 TMD from WSN. TMD interaction strengths were measured in the GALLEX system, where the association is proportional to the decrease in β-galactosidase activity. The relative TMD interaction strength was determined with respect to an empty-vector control. Error bars represent the standard deviation (SD) from three experiments, and the Student *t* test was used to calculate the significant differences from the WSN TMD (**, $P \leq 0.01$). Equal expression of the different NA TMD constructs was confirmed by immunoblotting. (C) The procedure for determining the NA folding efficiency at different temperatures based on the presence of the same enzymatic head domain. (D) Nonreducing (NR) and reducing (RD) immunoblots of the indicated NA constructs that were expressed in 293T cells at 33°C and 37°C for 48 h and standardized to their activity levels are shown. The resulting NA folding efficiencies displayed in panel E were determined by normalizing the activity levels in each sample to their total protein levels from the RD immunoblots. The values for NA^{WSN} expressed at 33°C were set to 100%, and the error bars represent the SD from three independent experiments.

ibility between these two domains is more important at warmer temperatures. To compensate for TMD-head domain incompatibility, H1N1 viruses modify the intrinsic amphipathic assembly of the TMD by preferentially introducing polar mutations. These mutations reestablish the N1 TMD-head domain compatibility by altering the intrinsic TMD association such that proper folding of the head domain is restored. Thus, it is likely that antigenic pressure on H1N1 viruses drives the selective evolution of the N1 head domain and results in subsequent changes in the TMD to maintain compatibility.

Disrupting the conserved N1 TMD assembly prevents viral replication at 37°C. Our results show that an old H1N1 virus containing the recent, more polar, and stronger-interacting pN1 TMD has impaired viral replication at 37°C that can be overcome by the selective introduction of further polar TMD mutations. Interestingly, all the observed mutations maintained the amphipathicity of the N1 TMD that is conserved in 100% of the 615 unique N1 TMD sequences from human, avian, and swine H1N1 viruses (Fig. 4A, polar *a* and *e* faces). Based on these observations, and the effects of the pN1 TMD exchange, we hypothesized that disrupting the N1 TMD amphipathicity would significantly impair H1N1 replication at 37°C.

To test this hypothesis, the NA segment in WSN was replaced with our previously engineered pN1 TMDΔA (21). In pN1 TMDΔA, Ala substitutions of the polar *a* face Asn residues at positions 21 and 28 create a less amphipathic and more hydrophobic TMD ($\Delta G_{app} = -1.4$ kcal/mol), with a decreased intrinsic association (Fig. 4B) (21). The examination of $WSN^{pN1\text{-}TMD\Delta A}$ replication following recovery by reverse genetics at 33°C and 37°C revealed that this virus was completely restricted to 33°C, where it showed slower replication than WSN (Fig. 4C). Viral particle isolation showed that the $WSN^{pN1\text{-}TMD\Delta A}$ virus had a substantial budding defect at 37°C, as no M1, and very little NP, was found at 37°C, whereas all were present in the particles isolated from 33°C (Fig. 4D). These results confirm our previous observation that the N1 TMD sequence and its assembly properties significantly affect IAV replication in a temperature-dependent manner.

Hydrophobic mutations in the nonamphipathic pN1 TMDΔA restore viral replication at 37°C. Due to the significant growth defect, it was not possible to generate $WSN^{pN1\text{-}TMD\Delta A}$ virus at 37°C by reverse genetics. Thus, the $WSN^{pN1\text{-}TMD\Delta A}$ virus recovered at 33°C was propagated at 37°C in an attempt to generate rescue mutations. In two separate trials, the temporal generation of infectious virus was followed over 3 days at 37°C (Fig. 5A). When the N1 TMDs were sequenced from the virus recovered at day 3, mixed mutational populations were seen for the codon of Met 19 in the TMD, and the signal for each mutation was proportional to the infectious titers (Fig. 5A, compare higher and lower titer chromatograms). These results show a direct correlation be-

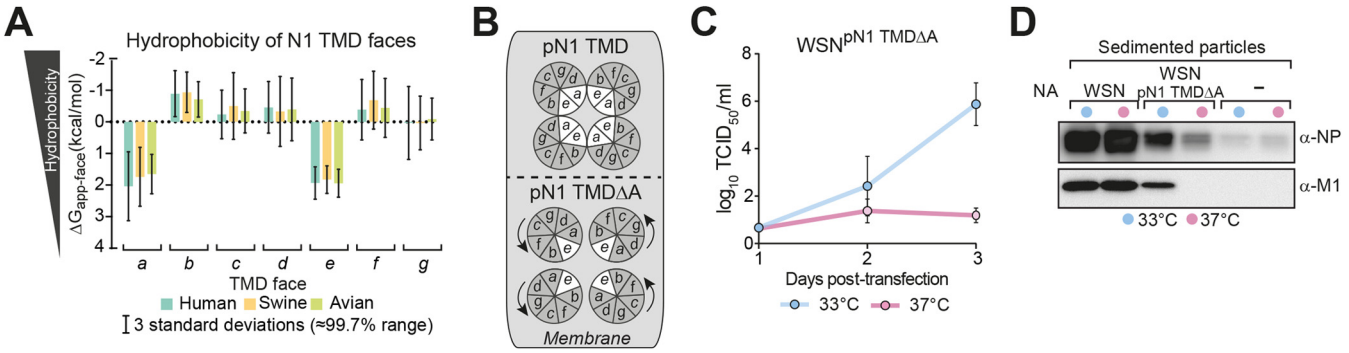

FIG 4 Disrupting the conserved amphipathic N1 TMD restricts viral replication to 33°C. (A) Graph displaying the conservation of the amphipathic characteristic (adjacent polar *a* and *e* faces with positive $\Delta G_{app\text{-}face}$ values) in 100% of the N1 TMDs from human, avian, and swine IAVs. (B) Proposed model of how mutating the polar *a* face residues (Asn 21 and Asn 28) in the pN1-TMDΔA to Ala alter its amphipathic assembly (white faces are polar). (C) Replication of $WSN^{pN1\text{-}TMD\Delta A}$ is restricted to 33°C. The graph displays mean viral titers ± SEM from three independent split transfections of $WSN^{pN1\text{-}TMD\Delta A}$ virus at 33°C and 37°C. (D) The indicated viral particles were isolated from the culture medium after 3 days of recovery at the indicated temperatures. The NP and M1 contents were determined by immunoblotting.

tween the mutation of Met 19 in the nonamphipathic pN1 TMDΔA and viral propagation at 37°C.

When the 33°C recovered $WSN^{pN1\text{-}TMD\Delta A}$ viruses were passaged twice at 37°C, three positionally conserved N1 TMD mutations (M19V, M19L, and M19I) had become fixed in the viral population (Fig. 5B). All these mutations are located toward the center of the membrane and increase the pN1 TMDΔA hydrophobicity, as the predicted ΔG_{app} value for membrane insertion went

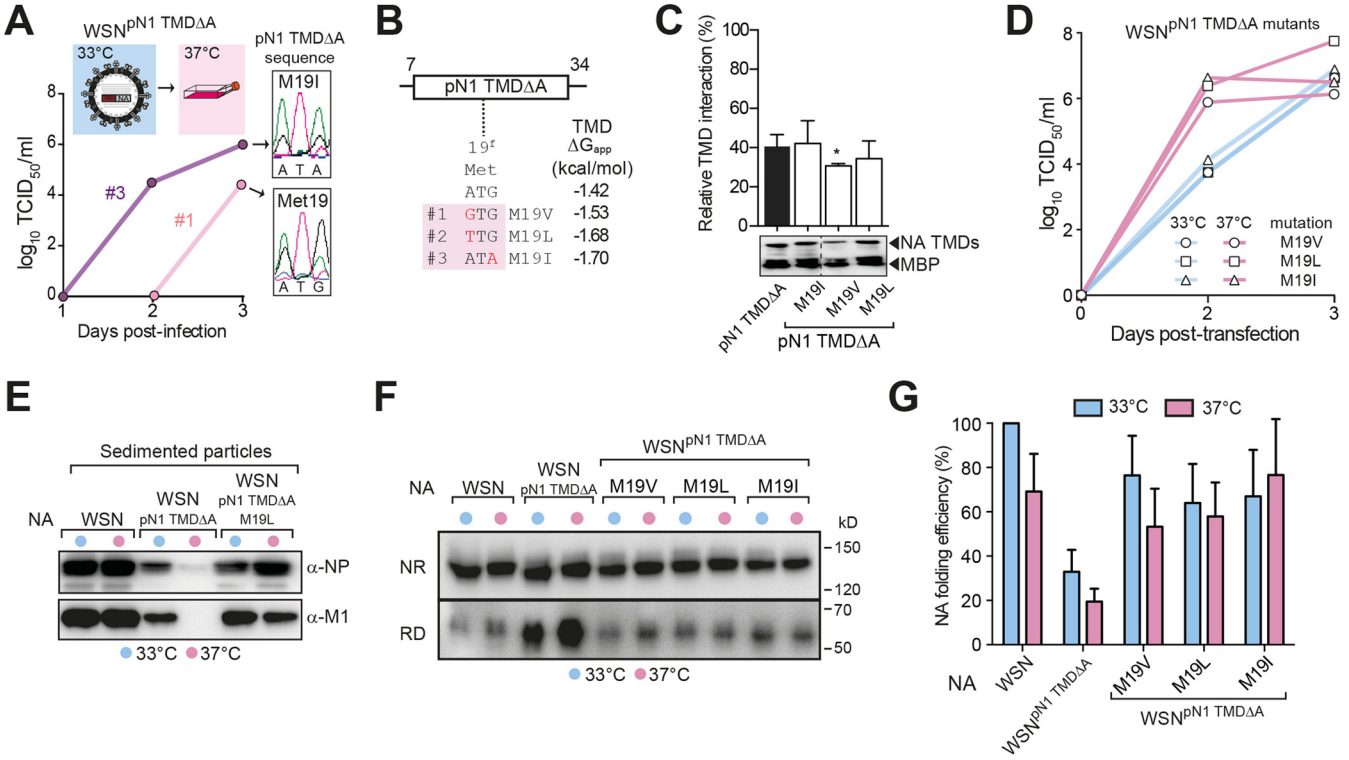

FIG 5 Hydrophobic N1 TMD mutations restore $WSN^{pN1\text{-}TMD\Delta A}$ replication at 37°C. (A) The pN1 TMDΔA mutations rescue $WSN^{pN1\text{-}TMD\Delta A}$ replication at 37°C. The graph displays the viral titers from two independent experiments where $WSN^{pN1\text{-}TMD\Delta A}$ virus that had been generated at 33°C was used to infect MDCK cells at 37°C using an MOI of ~0.001 that was determined at 33°C. Chromatograms show the mutations at Met 19 in the TMD at day 3. (B) The pN1 TMDΔA mutations at 37°C are all hydrophobic (ΔG_{app} values are more negative) and positionally conserved (Met 19). (C) The relative interaction strengths of the pN1 TMDΔA and the rescue mutations were determined as described for Fig. 3B. (D) The M19V, M19L, and M19I pN1 TMDΔA mutations were introduced into the $WSN^{pN1\text{-}TMD\Delta A}$ virus by reverse genetics, and each one rescued the replication at 37°C based on their viral titers at 33°C and 37°C. (E) The M1 and NP contents within the indicated viral particles that were isolated 3 days postrecovery are shown by the representative immunoblots. (F) Altering the N1 TMD amphipathicity significantly impairs the head domain folding, which is restored by the adaptive TMD mutations. Representative NR and RD immunoblots are shown of the indicated NA constructs expressed in 293T cells at 33°C and 37°C for 48 h and standardized to their activity levels. The resulting NA folding efficiencies displayed in panel G were performed as described for Fig. 3E.

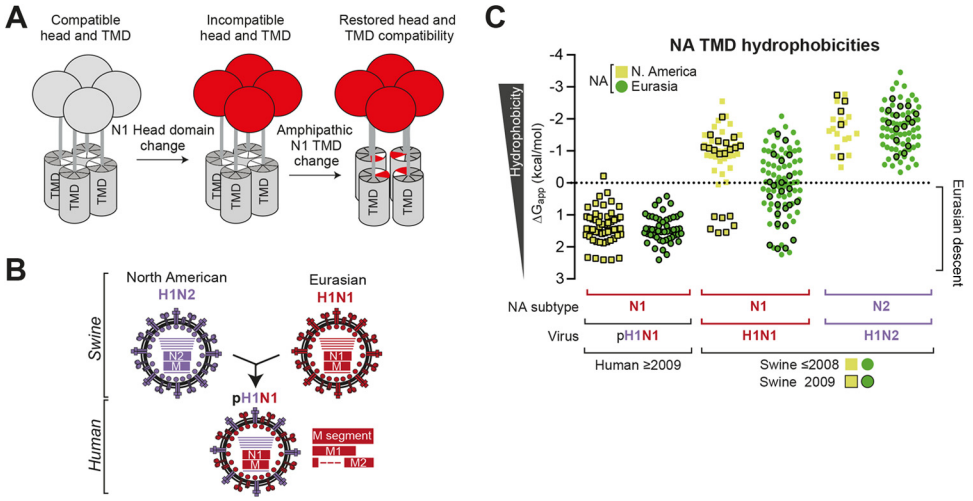

FIG 6 The Eurasian swine origin of the pN1 head domain can be traced by its low TMD hydrophobicity. (A) Model displaying how N1 head domain changes disrupt the folding compatibility with the N1 TMD. Head domain changes create selection pressure for residues (mainly polar) in the TMD that alter its amphipathic assembly and restore the compatibility. (B) Diagram showing the reassortment of the NA (N1 and N2) and M segments from geographically separated North American swine H1N2 viruses and the Eurasian swine H1N1 viruses that created the 2009 human pandemic pH1N1 virus. (C) Prior to 2009, the low N1 TMD hydrophobicity found in the pH1N1 viruses globally was present only in the swine H1N1 viruses from Eurasia (see "Swine ≤2008"). All the predicted N1 and N2 TMD hydrophobicities from the available swine (H1N1 and H1N2) and human pH1N1 viruses are displayed with respect to their geographic location and date of isolation (2009 and ≤2008).

from −1.4 kcal/mol to −1.7 kcal/mol. The different mutations did not consistently alter the pN1 TMDΔA association, likely because their associations are close to that of the WSN TMD, but it is possible that the mutations cause a TMD rearrangement that is not detected by this assay (Fig. 5C) (21). Similar mutations also appeared in the WSN$^{pN1\text{-}TMD\Delta A}$ virus after two passages at 33°C, suggesting that the NA folding defects are more severe and not completely suppressed at the permissive temperature.

To confirm that the N1 TMD mutations were directly responsible for the replication loss at 37°C, each of the mutations was introduced into the WSN$^{pN1\text{-}TMD\Delta A}$ background by reverse genetics, and their replication was analyzed at 33°C and 37°C. In all cases, the different Met 19 mutations restored virus replication at 37°C (Fig. 5D), and the isolated WSN$^{pN1\text{-}TMD\Delta A\ M19L}$ particles contained equivalent NP and M1 levels at 33°C and 37°C (Fig. 5E). These results support our previous finding that selection pressure exists on the N1 TMD and that this pressure is higher at temperatures ≥37°C. In contrast to the amphipathic pN1 TMD that was rescued by polar mutations, the hydrophobic nonamphipathic pN1 TMDΔA was rescued by hydrophobic mutations. Thus, the requirement for NA TMD compatibility exerts selective pressure that is alleviated by property-dependent TMD adaptation.

Hydrophobic mutations rescue the nonamphipathic TMD-related NA folding defects. Similar to the WSN$^{pN1\text{-}TMD}$ NA chimera, the folding efficiency of the WSN$^{pN1\text{-}TMD\Delta A}$ NA chimera was better at 33°C than at 37°C but still quite inefficient at 33°C (Fig. 5F and G). This difference likely explains why the pN1 TMDΔA rescue mutations that were required for viral replication at 37°C also appeared after only two passages at 33°C. In line with our previous observations, all of the viral selected mutations in the pN1 TMDΔA (M19V, M19L, and M19I) also restored the NA folding efficiency at both 33°C and 37°C. These results demonstrate by a second approach that folding of the N1 head domain is TMD and temperature dependent, that poor NA folding impairs viral budding, and that the compatibility requirement between these two domains increases with temperature. The comparative analysis of the different NA TMD sequences that are compatible with the WSN head domain revealed that the NA TMD has substantial plasticity, and, in viruses, this plasticity is restricted by the intrinsic assembly properties of the TMD.

DISCUSSION

The findings presented here show the importance of TMDs from single-spanning membrane proteins, as changes to the TMD can cause subtle defects in distal domains that can profoundly affect the biological function of the protein. More specifically, our results demonstrate that a compatibility requirement exists between the NA TMD and its distal enzymatic head domain in H1N1 viruses that is linked to the folding efficiency of NA. Changes in either the NA TMD or head domain that disrupt their compatibility result in NA folding defects that are reflected by a deficiency in the viral budding and replication process. This relationship forms a significant fitness barrier, which explains why the N1 TMDs have only modified their conserved amphipathic assembly. Furthermore, the mutagenic selection during the viral replication process revealed the plasticity of the NA TMD sequences that support head domain folding and confirmed that their compatibility is critical for viral replication.

Our results are summarized by a model which illustrates how the subtype 1 NA TMD and head domain have coevolved (Fig. 6A). In this model, changes in the N1 head domain, presumably to mask antigenic epitopes, disrupt the folding compatibility with the existing TMD. During replication, the N1 head domain drives the biased selection of polar TMD mutations, which modify the intrinsic amphipathic TMD assembly to restore compatibility with the head domain. This likely explains why the N1 TMDs have become more polar as the head domain has changed at both the sequence and enzymatic levels (22).

The pN1 TMD used in this study is from the human 2009 pH1N1 virus and is associated with a head domain of novel antigenicity (41). The N1 and M segments (of pH1N1) originated from a Eurasian swine H1N1 virus, and together these replaced the N2 and M segments in a North American swine H1N2 to create the pH1N1 virus (Fig. 6B) (29). To further test if H1N1 viruses need to maintain the NA TMD and head domain compatibility, we tracked the Eurasian swine origin of the pN1 head domain by the low hydrophobicity ($\Delta G_{app} > 0$ kcal/mol) of its TMD (Fig. 6C, pH1N1). Upon sorting all N1 and N2 swine IAV sequences geographically and by date, the only NA TMDs with low hydrophobicity prior to 2009 (swine ≤2008) were from Eurasian swine H1N1 viruses (Fig. 6C). The NA TMDs in the North American swine H1N1 IAVs showed low hydrophobicity only in 2009, when this trait also surfaced in the human population, and all of the N2 TMDs remained hydrophobic. The ability to trace the origin of the pN1 segment by the properties of its TMD further supports the link between the N1 TMD and head domain.

Previous studies have shown that TMDs from single-spanning membrane proteins assemble by multiple mechanisms, which include hydrogen bonding and hydrophobic and charge-charge interactions (42–45). By comparing the properties of the viral selected mutations in the strong-interacting pN1 TMD and the moderate-interacting pN1 TMDΔA (21), a trend in their functional plasticity was found. The natural polar-amphipathic pN1 TMD showed a preference to select for polar residues in a variety of positions during adaptation at 37°C. Two of these pN1 TMD mutants were also found in natural pH1N1 viruses from 2011, indicating our approach likely generates natural TMD adaptations. In the hydrophobic pN1 TMDΔA, the selection preference switched to hydrophobic residues in a conserved position. Based on these observations, it appears the N1 TMD has substantial functional plasticity that is restricted by its inherent mechanism of association.

The functional roles of TMD interactions in single-spanning eukaryotic membrane proteins have been linked mainly to homo- and heterocomplex assembly (5, 6, 9, 46, 47). Here, we found that the TMD contributes to the folding efficiency of the distal N1 head domain in a temperature-dependent manner. Consequently, changes in the NA TMD and temperature both influenced viral replication and caused the selection of mutations that largely restored the NA folding efficiency. These findings may explain previously reported impairments in IAV replication that resulted from alanine scanning mutagenesis of the N1 TMD and the exchange of NA TMDs from different H1N1 or influenza B viruses (48–50).

For the pN1 TMD, the selected mutations both enhanced the NA folding efficiency and changed the TMD association in a measurable manner by the GALLEX assay. However, none of the Met 19 mutations in the pN1 TMDΔA altered its association in any obvious pattern, yet they all enhanced the NA folding efficiency. One possible explanation for the lack of a detectable change in the TMD association is how the GALLEX system works (27). NA TMDs independently exist as tetramers in both mammalian and *E. coli* membranes, and the assay cannot discriminate between dimers and tetramers (20, 21), and it is not known how changes in these two states would affect the assay. Another explanation could be a change in the TMD assembly orientation but not the affinity. The TMD orientation change could stress the head domain assembly via the stalk, which could negatively impact the NA head domain tetramerization that is required for function. Since compensatory mutations were also picked up in the NA head domain with the pN1 TMD chimera, this appears to be a likely scenario, but more detailed studies are required.

Differences in viral replication, due to the TMD-mediated decreases in the NA folding efficiency, were attributed to defects in viral budding or release. This conclusion was based on the decrease or absence of the viral core components NP and M1 following the sedimentation of the cell culture medium. For $WSN^{pN1\text{-}TMD\Delta A}$, the data were rather straightforward, infectious particles were present at 33°C but not at 37°C, and particles containing M1 and NP could be isolated only from the cells at 33°C. However, for $WSN^{pN1\text{-}TMD}$, a similar pattern was observed even though infectious particles are present at both temperatures. One difference is that detectable amounts of NA activity were observed in the $WSN^{pN1\text{-}TMD}$ particles isolated at both temperatures that reflected their infectious titer values. Thus, the incompatibility of the NA TMD may also affect the proposed N-terminal tail recruitment of M1 and subsequently NP (51), but this is speculative, and more directed experiments are required to validate any effects on M1 recruitment.

Examination of the N1 TMD revealed two different barriers for adaptation. The first is a requirement for TMD association strength to be compatible with the folding requirements of the head domain. The second is the requirement that the resulting conformation is adapted to the hydrophobic membrane environment. However, the amphipathic N1 and hydrophobic N2 TMD properties are conserved in human influenza viruses (21). This conservation suggests that the dual fitness cost associated with dramatically altering the TMD assembly and adapting the new conformation to the membrane is too high to overcome, resulting in the two distinct property lineages.

In summary, our results indicate that significant selection pressure exists on N1 TMDs to retain compatibility with their head domains. Even subtle head domain folding defects due to a nonoptimal TMD severely impaired IAV replication. This observation revealed an unexpected role of a viral TMD in pathogenesis and illustrates the need to study membrane protein TMDs in native biological systems. Previous findings have shown that the majority of "NA-less" viruses still carry the NA TMD; thus, it is possible the TMD effect we observed is also due to critical lipid or protein interactions that facilitate viral assembly and budding (52–54). Thus, future studies are needed to investigate the involvement of lipids, membrane composition, and membrane-associated proteins in the function of the NA TMD and the TMDs from eukaryotic bitopic proteins.

ACKNOWLEDGMENTS

We are indebted to Jan Willem de Gier for his insightful suggestions and critique of the manuscript and the Center for Biomembrane Research members for their discussions.

This work was supported by grants from the Swedish Research Council, Swedish Foundation for Strategic Research, Carl Trygger Foundation, and Harald Jeanssons Stiftelse to R.D., from Helge Ax:Son Johnsons and Lindhés Advokatbyrå AB to D.V.D.S. and J.N., and from the Sven and Lilly Lawskis Fund to J.N.

We declare that no competing financial interests exist.

REFERENCES

1. **Li E, Wimley WC, Hristova K.** 2012. Transmembrane helix dimerization: beyond the search for sequence motifs. Biochim Biophys Acta **1818:** 183–193. http://dx.doi.org/10.1016/j.bbamem.2011.08.031.
2. **Langosch D, Arkin IT.** 2009. Interaction and conformational dynamics of membrane-spanning protein helices. Protein Sci **18:**1343–1358. http://dx.doi.org/10.1002/pro.154.
3. **Moore DT, Berger BW, DeGrado WF.** 2008. Protein-protein interactions in the membrane: sequence, structural, and biological motifs. Structure **16:**991–1001. http://dx.doi.org/10.1016/j.str.2008.05.007.
4. **Shaw AC, Mitchell RN, Weaver YK, Campos-Torres J, Abbas AK, Leder P.** 1990. Mutations of immunoglobulin transmembrane and cytoplasmic domains: effects on intracellular signaling and antigen presentation. Cell **63:**381–392. http://dx.doi.org/10.1016/0092-8674(90)90171-A.
5. **Call ME, Pyrdol J, Wiedmann M, Wucherpfennig KW.** 2002. The organizing principle in the formation of the T cell receptor-CD3 complex. Cell **111:**967–979. http://dx.doi.org/10.1016/S0092-8674(02)01194-7.
6. **Lilley BN, Tortorella D, Ploegh HL.** 2003. Dislocation of a type I membrane protein requires interactions between membrane-spanning segments within the lipid bilayer. Mol Biol Cell **14:**3690–3698. http://dx.doi.org/10.1091/mbc.E03-03-0192.
7. **Li R, Mitra N, Gratkowski H, Vilaire G, Litvinov R, Nagasami C, Weisel JW, Lear JD, DeGrado WF, Bennett JS.** 2003. Activation of integrin alphaIIb beta3 by modulation of transmembrane helix associations. Science **300:**795–798. http://dx.doi.org/10.1126/science.1079441.
8. **Luo BH, Carman CV, Takagi J, Springer TA.** 2005. Disrupting integrin transmembrane domain heterodimerization increases ligand binding affinity, not valency or clustering. Proc Natl Acad Sci U S A **102:**3679–3684. http://dx.doi.org/10.1073/pnas.0409440102.
9. **Feige MJ, Hendershot LM.** 2013. Quality control of integral membrane proteins by assembly-dependent membrane integration. Mol Cell **51:**297–309. http://dx.doi.org/10.1016/j.molcel.2013.07.013.
10. **Grove J, Marsh M.** 2011. The cell biology of receptor-mediated virus entry. J Cell Biol **195:**1071–1082. http://dx.doi.org/10.1083/jcb.201108131.
11. **Marsh M, Helenius A.** 2006. Virus entry: open sesame. Cell **124:**729–740. http://dx.doi.org/10.1016/j.cell.2006.02.007.
12. **Pelkmans L, Helenius A.** 2003. Insider information: what viruses tell us about endocytosis. Curr Opin Cell Biol **15:**414–422. http://dx.doi.org/10.1016/S0955-0674(03)00081-4.
13. **Daniels R, Kurowski B, Johnson AE, Hebert DN.** 2003. N-linked glycans direct the cotranslational folding pathway of influenza hemagglutinin. Mol Cell **11:**79–90. http://dx.doi.org/10.1016/S1097-2765(02)00821-3.
14. **White JM, Delos SE, Brecher M, Schornberg K.** 2008. Structures and mechanisms of viral membrane fusion proteins: multiple variations on a common theme. Crit Rev Biochem Mol Biol **43:**189–219. http://dx.doi.org/10.1080/10409230802058320.
15. **Dutch RE, Jardetzky TS, Lamb RA.** 2000. Virus membrane fusion proteins: biological machines that undergo a metamorphosis. Biosci Rep **20:** 597–612. http://dx.doi.org/10.1023/A:1010467106305.
16. **Gottschalk A.** 1957. Neuraminidase: the specific enzyme of influenza virus and *Vibrio cholerae*. Biochim Biophys Acta **23:**645–646. http://dx.doi.org/10.1016/0006-3002(57)90389-X.
17. **Palese P, Compans RW.** 1976. Inhibition of influenza virus replication in tissue culture by 2-deoxy-2,3-dehydro-*N*-trifluoroacetylneuraminic acid (FANA): mechanism of action. J Gen Virol **33:**159–163. http://dx.doi.org/10.1099/0022-1317-33-1-159.
18. **Bos TJ, Davis AR, Nayak DP.** 1984. NH2-terminal hydrophobic region of influenza virus neuraminidase provides the signal function in translocation. Proc Natl Acad Sci U S A **81:**2327–2331. http://dx.doi.org/10.1073/pnas.81.8.2327.
19. **Laver WG.** 1978. Crystallization and peptide maps of neuraminidase "heads" from H2N2 and H3N2 influenza virus strains. Virology **86:**78–87. http://dx.doi.org/10.1016/0042-6822(78)90009-0.
20. **da Silva DV, Nordholm J, Madjo U, Pfeiffer A, Daniels R.** 2013. Assembly of subtype 1 influenza neuraminidase is driven by both the transmembrane and head domains. J Biol Chem **288:**644–653. http://dx.doi.org/10.1074/jbc.M112.424150.
21. **Nordholm J, da Silva DV, Damjanovic J, Dou D, Daniels R.** 2013. Polar residues and their positional context dictate the transmembrane domain interactions of influenza a neuraminidases. J Biol Chem **288:**10652–10660. http://dx.doi.org/10.1074/jbc.M112.440230.
22. **Yen HL, Liang CH, Wu CY, Forrest HL, Ferguson A, Choy KT, Jones J, Wong DD, Cheung PP, Hsu CH, Li OT, Yuen KM, Chan RW, Poon LL, Chan MC, Nicholls JM, Krauss S, Wong CH, Guan Y, Webster RG, Webby RJ, Peiris M.** 2011. Hemagglutinin-neuraminidase balance confers respiratory-droplet transmissibility of the pandemic H1N1 influenza virus in ferrets. Proc Natl Acad Sci U S A **108:**14264–14269. http://dx.doi.org/10.1073/pnas.1111000108.
23. **Hoffmann E, Neumann G, Kawaoka Y, Hobom G, Webster RG.** 2000. A DNA transfection system for generation of influenza A virus from eight plasmids. Proc Natl Acad Sci U S A **97:**6108–6113. http://dx.doi.org/10.1073/pnas.100133697.
24. **Mellroth P, Daniels R, Eberhardt A, Ronnlund D, Blom H, Widengren J, Normark S, Henriques-Normark B.** 2012. LytA, major autolysin of *Streptococcus pneumoniae*, requires access to nascent peptidoglycan. J Biol Chem **287:**11018–11029. http://dx.doi.org/10.1074/jbc.M111.318584.
25. **Reed LJ, Muench H.** 1938. A simple method of estimating fifty percent end points. Am J Epidemiol **27:**493–497.
26. **Francis E, Daniels R, Hebert DN.** 2002. Analysis of protein folding and oxidation in the endoplasmic reticulum. Curr Protoc Cell Biol **Chapter 15:**Unit 15.6.
27. **Schneider D, Engelman DM.** 2003. GALLEX, a measurement of heterologous association of transmembrane helices in a biological membrane. J Biol Chem **278:**3105–3111. http://dx.doi.org/10.1074/jbc.M206287200.
28. **Hessa T, Meindl-Beinker NM, Bernsel A, Kim H, Sato Y, Lerch-Bader M, Nilsson I, White SH, von Heijne G.** 2007. Molecular code for transmembrane-helix recognition by the Sec61 translocon. Nature **450:**1026–1030. http://dx.doi.org/10.1038/nature06387.
29. **Morens DM, Taubenberger JK, Fauci AS.** 2009. The persistent legacy of the 1918 influenza virus. N Engl J Med **361:**225–229. http://dx.doi.org/10.1056/NEJMp0904819.
30. **Palese P, Tobita K, Ueda M, Compans RW.** 1974. Characterization of temperature sensitive influenza virus mutants defective in neuraminidase. Virology **61:**397–410. http://dx.doi.org/10.1016/0042-6822(74)90276-1.
31. **Bos TJ, Nayak DP.** 1986. Identification of defects in the neuraminidase gene of four temperature-sensitive mutants of A/WSN/33 influenza virus. Virology **154:**85–96. http://dx.doi.org/10.1016/0042-6822(86)90432-0.
32. **Basler CF, Garcia-Sastre A, Palese P.** 1999. Mutation of neuraminidase cysteine residues yields temperature-sensitive influenza viruses. J Virol **73:**8095–8103.
33. **Sugiura A, Tobita K, Kilbourne ED.** 1972. Isolation and preliminary characterization of temperature-sensitive mutants of influenza virus. J Virol **10:**639–647.
34. **Mitnaul LJ, Matrosovich MN, Castrucci MR, Tuzikov AB, Bovin NV, Kobasa D, Kawaoka Y.** 2000. Balanced hemagglutinin and neuraminidase activities are critical for efficient replication of influenza A virus. J Virol **74:** 6015–6020. http://dx.doi.org/10.1128/JVI.74.13.6015-6020.2000.
35. **Kaverin NV, Gambaryan AS, Bovin NV, Rudneva IA, Shilov AA, Khodova OM, Varich NL, Sinitsin BV, Makarova NV, Kropotkina EA.** 1998. Postreassortment changes in influenza A virus hemagglutinin restoring HA-NA functional match. Virology **244:**315–321. http://dx.doi.org/10.1006/viro.1998.9119.
36. **Kaverin NV, Matrosovich MN, Gambaryan AS, Rudneva IA, Shilov AA, Varich NL, Makarova NV, Kropotkina EA, Sinitsin BV.** 2000. Intergenic HA-NA interactions in influenza A virus: postreassortment substitutions of charged amino acid in the hemagglutinin of different subtypes. Virus Res **66:**123–129. http://dx.doi.org/10.1016/S0168-1702(99)00131-8.
37. **Sugrue RJ, Bahadur G, Zambon MC, Hall-Smith M, Douglas AR, Hay AJ.** 1990. Specific structural alteration of the influenza haemagglutinin by amantadine. EMBO J **9:**3469–3476.
38. **Steinhauer DA, Wharton SA, Skehel JJ, Wiley DC, Hay AJ.** 1991. Amantadine selection of a mutant influenza virus containing an acid-stable hemagglutinin glycoprotein: evidence for virus-specific regulation of the pH of glycoprotein transport vesicles. Proc Natl Acad Sci U S A **88:**11525–11529. http://dx.doi.org/10.1073/pnas.88.24.11525.
39. **Dou D, da Silva DV, Nordholm J, Wang H, Daniels R.** 2014. Type II transmembrane domain hydrophobicity dictates the cotranslational dependence for inversion. Mol Biol Cell **25:**3363–3374. http://dx.doi.org/10.1091/mbc.E14-04-0874.
40. **Cao Z, Bowie JU.** 2012. Shifting hydrogen bonds may produce flexible transmembrane helices. Proc Natl Acad Sci U S A **109:**8121–8126. http://dx.doi.org/10.1073/pnas.1201298109.
41. **Li Q, Qi J, Zhang W, Vavricka CJ, Shi Y, Wei J, Feng E, Shen J, Chen J, Liu D, He J, Yan J, Liu H, Jiang H, Teng M, Li X, Gao GF.** 2010. The

2009 pandemic H1N1 neuraminidase N1 lacks the 150-cavity in its active site. Nat Struct Mol Biol **17:**1266–1268. http://dx.doi.org/10.1038/nsmb.1909.
42. **Gratkowski H, Lear JD, DeGrado WF.** 2001. Polar side chains drive the association of model transmembrane peptides. Proc Natl Acad Sci U S A **98:**880–885. http://dx.doi.org/10.1073/pnas.98.3.880.
43. **Zhou FX, Cocco MJ, Russ WP, Brunger AT, Engelman DM.** 2000. Interhelical hydrogen bonding drives strong interactions in membrane proteins. Nat Struct Biol **7:**154–160. http://dx.doi.org/10.1038/72430.
44. **Cosson P, Lankford SP, Bonifacino JS, Klausner RD.** 1991. Membrane protein association by potential intramembrane charge pairs. Nature **351:**414–416. http://dx.doi.org/10.1038/351414a0.
45. **Ridder A, Skupjen P, Unterreitmeier S, Langosch D.** 2005. Tryptophan supports interaction of transmembrane helices. J Mol Biol **354:**894–902. http://dx.doi.org/10.1016/j.jmb.2005.09.084.
46. **Schneider D, Engelman DM.** 2004. Involvement of transmembrane domain interactions in signal transduction by alpha/beta integrins. J Biol Chem **279:**9840–9846. http://dx.doi.org/10.1074/jbc.M312749200.
47. **Yang J, Ma YQ, Page RC, Misra S, Plow EF, Qin J.** 2009. Structure of an integrin alphaIIb beta3 transmembrane-cytoplasmic heterocomplex provides insight into integrin activation. Proc Natl Acad Sci U S A **106:**17729–17734. http://dx.doi.org/10.1073/pnas.0909589106.
48. **Jing X, Phy K, Li X, Ye Z.** 2012. Increased hemagglutinin content in a reassortant 2009 pandemic H1N1 influenza virus with chimeric neuraminidase containing donor A/Puerto Rico/8/34 virus transmembrane and stalk domains. Vaccine **30:**4144–4152. http://dx.doi.org/10.1016/j.vaccine.2012.04.073.
49. **Barman S, Adhikary L, Chakrabarti AK, Bernas C, Kawaoka Y, Nayak DP.** 2004. Role of transmembrane domain and cytoplasmic tail amino acid sequences of influenza A virus neuraminidase in raft association and virus budding. J Virol **78:**5258–5269. http://dx.doi.org/10.1128/JVI.78.10.5258-5269.2004.
50. **Flandorfer A, Garcia-Sastre A, Basler CF, Palese P.** 2003. Chimeric influenza A viruses with a functional influenza B virus neuraminidase or hemagglutinin. J Virol **77:**9116–9123. http://dx.doi.org/10.1128/JVI.77.17.9116-9123.2003.
51. **Rossman JS, Lamb RA.** 2011. Influenza virus assembly and budding. Virology **411:**229–236. http://dx.doi.org/10.1016/j.virol.2010.12.003.
52. **Liu C, Air GM.** 1993. Selection and characterization of a neuraminidase-minus mutant of influenza virus and its rescue by cloned neuraminidase genes. Virology **194:**403–407. http://dx.doi.org/10.1006/viro.1993.1276.
53. **Yang P, Bansal A, Liu C, Air GM.** 1997. Hemagglutinin specificity and neuraminidase coding capacity of neuraminidase-deficient influenza viruses. Virology **229:**155–165. http://dx.doi.org/10.1006/viro.1996.8421.
54. **Gubareva LV, Nedyalkova MS, Novikov DV, Murti KG, Hoffmann E, Hayden FG.** 2002. A release-competent influenza A virus mutant lacking the coding capacity for the neuraminidase active site. J Gen Virol **83:**2683–2692.